ORIGINAL PAPER

THE LID-DRIVEN HYDROMAGNETIC FLOW OF NEWTONIAN AND NON-NEWTONIAN LIQUIDS IN A SQUARE CAVITY

SERPİL SAHİN[1], HÜSEYİN DEMİR[2]

Manuscript received: 11.01.2021; Accepted paper: 28.09.2021;
Published online: 30.09.2021.

Abstract. *In this paper, we formulate the steady hydromagnetic lid-driven cavity problem in a stream function-vorticity form for weakly electrically conducting Newtonian and non-Newtonian liquids. Then we solve them by using the concept of pseudo time derivative. The classical benchmark results of the Newtonian liquid are recovered as a limiting case and the inhibiting influence of the magnetic field on the Newtonian and non-Newtonian liquids' flow field is clearly depicted through graphs. We also show certain aspects of the flow for the first time in tables.*

Keywords: *pseudo time derivative*; *hydromagnetics*; *lid-driven cavity flow*; *Newtonian liquid*; *non-Newtonian liquid.*

1. INTRODUCTION

The interest in magnetohydrodynamics (MHD) flow has begun in 1907 when Northrop built an MHD pump prototype. Since then, the analysis of the effects of both rotation and magnetic fields on fluid flows has been an active research area. The system of MHD equations is a coupled equation system of Navier-Stokes equations of fluid dynamics and Maxwell's equations of electromagnetism via Lorentz's force and Ohm's law. MHD is a branch of science studying the dynamics of electrically conducting fluids in the presence of electromagnetic field. Because of its applications in engineering such as liquid-metal cooling of nuclear reactors, solar technologies, crystal growth in liquids and electromagnetic casting, etc. it is usually regarded as a very up to the date subject. The work of Chandrasekhar [1], Danielson [2] and Unno [3] showed that the results of the magnetoconvection problem can be useful in the study of sunspot as well as penumbral convections. However, it must be emphasized that the magnetoconvection problem is required in the first step studies of the application problems mentioned above.

Numerical methods are frequently used for two dimensional steady incompressible Newtonian and non-Newtonian flow problems. Due to the simplicity of cavity geometry, numerical methods can be applied easily and effectively to this type of flow problems, and the results are very satisfactory. To this purpose, Benjamin and Denny [4] used a method that is relaxed by means of Alternating Direction Implicit (ADI) methods using a non-uniform iteration parameter. Full converged solutions at Reynolds number up to 10^4 with three different grid mesh sizes (maximum being 101×101) were generated in order to resolve basic questions on the nature of the flow and to explore convergence properties of the method.

[1] Amasya University, Faculty of Arts and Sciences, Department of Mathematics, 05000, Amasya, Turkey.
E-mail: serpil.sahin@amasya.edu.tr ; serpilsah55@gmail.com
[2] Samsun Unıversity, Faculty of Engineerıng, Software Engineering, 55420, Samsun, Turkey.
E-mail: huseyin.demir@samsun.edu.tr

Schereiber and Keller [5] introduced efficient and reliable numerical techniques with high-order accuracy for solving problems of steady viscous incompressible flow in the plane. They obtained accurate solutions for the driven cavity. For nonlinear systems, they combined numerical methods with an efficient linear system solver and an adaptive Newton-like method resulting solutions at Reynolds number 10000 on a 180×180 grid.

Hou et al. [6] used the Lattice Boltzmann Method for the simulation of cavity flow. In their work, approximate solutions for Reynolds number $\mathrm{Re} \le 7500$ were presented.

Liao and Zhu [7] introduced a higher order stream function-vorticity boundary element method (BEM) formulation for the solution of Navier-Stokes equations. They presented solutions up to $\mathrm{Re} = 10000$ with a grid mesh of 257×257.

Ghia et al. [8] applied a multi-grid strategy to the coupled strongly implicit method developed by Rubin and Khosla [9]. They presented solutions for Reynolds number as high as $\mathrm{Re} = 10000$ with meshes consisting of as many as 257×257 grid points.

Erturk et al. [10] introduced an effective numerical method for driven cavity flow by using stream function and vorticity formulation. Using the regular grid size of 601×601, they solved the Navier-Stokes equations for $\mathrm{Re} \le 21000$.

In the last decades, various numerical approaches have been used to solve MHD flows. A mixed finite element method was studied by Gunzburger et al. [11]. In [12], a weighted regularization approach was applied to incompressible MHD systems. Salama [13] studied the two-dimensional non-Newtonian steady flow on a power-law stretched surface with suction or injection. Siddheswar et al. [14] introduced the higher order Rayleigh-Ritz (HORR) method that is used to obtain the critical eigenvalues in the problem. Raisi et al. [15] introduced a numerical study of forced convection between hot and cold nanofluid laminar flows separated by a thin membrane in a horizontal channel. Venkatachalappa et al. [16] used ADI and Successive Line Over Relaxation (SLOR) method. Hasanpour et al. [17] used the Lattice Boltzman method to study the Prandtl number effect on flow structure and heat transfer rates in a MHD flow mixed convection in a lid-driven cavity filled with a porous medium. Mirza et al. [18] used a magneto-hydrodynamic approach to study the non-Newtonian blood flow, together with magnetic particles in a stenosed artery. Aydin et al. [19] reported a stabilized sub-grid method with two level finite element method.

Additionally, three classical iterative algorithms (Stokes iterative method, Newton iterative method and Oseen iterative method) for solving 2D/3D Navier Stokes equations were considered by He and Li [20], Xu and He [21].

One of the most important spatially factorized schemes is the Beam and Warming method that formulates the equations in delta (Δ) form. The advantage of this method is that the second-order (Δt^2) terms occuring due to the factorization do not appear at the steady-state. However, second-order terms appear at the steady-state in the formulation of [10]. This problem is overcomed by adding Δt^2 terms to the right side of the equation. In addition, there is a Δt term in the delta (Δ) formulation of the vorticity equation. However, this term does not exist in [10]. Instead, cross derivatives of Δt^2 order terms appear on the right side of the equation. Since Δt is small, Δt^2 is smaller. Thus, the formulation in [10] is more effective than the delta (Δ) formulation. For these reasons, the formulation in [10] was used in this study.

In this study, we compare the results when a magnetic field acts on the flow with the results in the absence of a magnetic field in upper wall moving flow. In this sense, our study investigates Chandrasekhar number effect on flow structure in a lid-driven cavity.

2. NUMERICAL METHOD

We consider the flow in a lid-driven cavity region. Schematical representation with boundary conditions is given in Fig. 1. In this case $\omega_L, \omega_R, \omega_B, \omega_T$ are given.

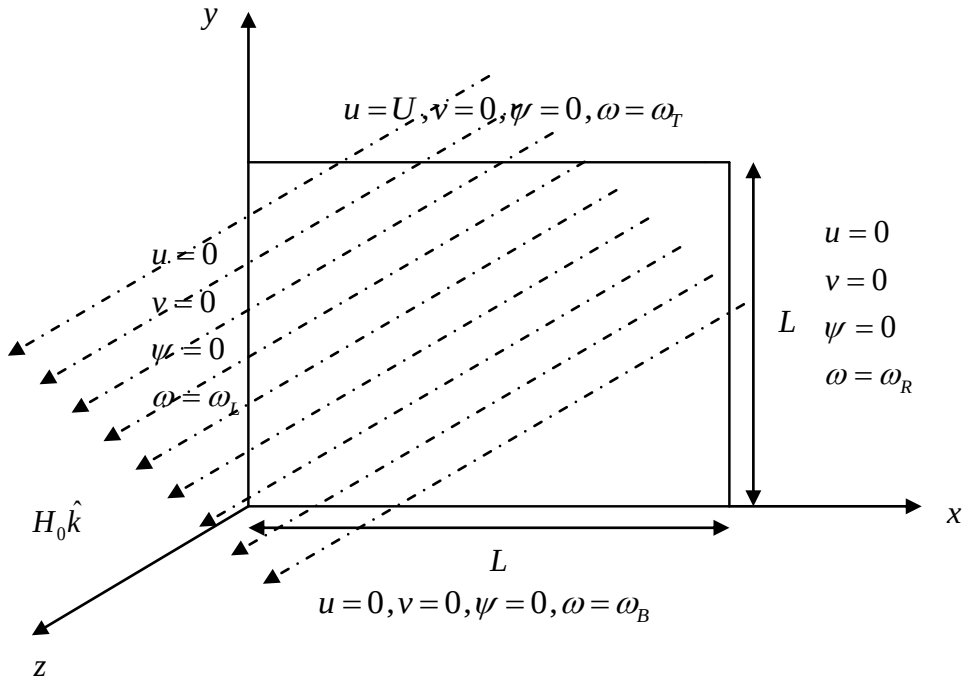

Figure 1. Physical configuration and description of boundary conditions.

2.1. NEWTONIAN CASE

We use the stream function (ψ) and vorticity (ω) formulation for the lid-driven flow of an electrically conducting Newtonian fluid. It has the form

$$\frac{\partial^2 \psi}{\partial x^2} + \frac{\partial^2 \psi}{\partial y^2} = -\omega, \tag{1}$$

$$\frac{\partial \psi}{\partial y}\frac{\partial \omega}{\partial x} - \frac{\partial \psi}{\partial x}\frac{\partial \omega}{\partial y} = \frac{1}{\mathrm{Re}}\left(\frac{\partial^2 \omega}{\partial x^2} + \frac{\partial^2 \omega}{\partial y^2}\right) - Q\omega, \tag{2}$$

where $\mathrm{Re} = \dfrac{UL}{\nu}$ is the Reynolds number, $Q = \dfrac{\mu_m^2 \sigma H_0^2 L}{u\rho}$ is the Chandrasekhar number, and x and y are the Cartesian coordinates as shown in Fig. 1. By introducing the first order pseudo time derivatives into the equations (1) and (2), we get the following:

$$\frac{\partial \psi}{\partial t} = \frac{\partial^2 \psi}{\partial x^2} + \frac{\partial^2 \psi}{\partial y^2} + \omega, \tag{3}$$

$$\frac{\partial \omega}{\partial t}=\frac{1}{\mathrm{Re}}\frac{\partial^2 \omega}{\partial x^2}+\frac{1}{\mathrm{Re}}\frac{\partial^2 \omega}{\partial y^2}+\frac{\partial \psi}{\partial x}\frac{\partial \omega}{\partial y}-\frac{\partial \psi}{\partial y}\frac{\partial \omega}{\partial x}-Q\omega\,. \tag{4}$$

We will approximate these equations with respect to *t*. Using forward difference approximation [29] for the time derivatives in equations (3) and (4), we obtain the following equations:

$$\left(1-\Delta t\frac{\partial^2}{\partial x^2}-\Delta t\frac{\partial^2}{\partial y^2}\right)\psi^{n+1}=\psi^n+\Delta t\omega^n\,, \tag{5}$$

$$\left(1-\frac{\Delta t}{\mathrm{Re}}\frac{\partial^2}{\partial x^2}-\frac{\Delta t}{\mathrm{Re}}\frac{\partial^2}{\partial y^2}-\Delta t\left(\frac{\partial \psi}{\partial x}\right)^n\frac{\partial}{\partial y}+\Delta t\left(\frac{\partial \psi}{\partial y}\right)^n\frac{\partial}{\partial x}\right)\omega^{n+1}=\omega^n-\Delta tQ\omega^n\,. \tag{6}$$

Since Δt is quite small, we can spatially factorize equations (5) and (6) as follows:

$$\left(1-\Delta t\frac{\partial^2}{\partial x^2}\right)\left(1-\Delta t\frac{\partial^2}{\partial y^2}\right)\psi^{n+1}=\psi^n+\Delta t\omega^n\,, \tag{7}$$

$$\left(1-\frac{\Delta t}{\mathrm{Re}}\frac{\partial^2}{\partial x^2}+\Delta t\left(\frac{\partial \psi}{\partial y}\right)^n\frac{\partial}{\partial x}\right)\left(1-\frac{\Delta t}{\mathrm{Re}}\frac{\partial^2}{\partial y^2}-\Delta t\left(\frac{\partial \psi}{\partial x}\right)^n\frac{\partial}{\partial y}\right)\omega^{n+1}=\omega^n-\Delta tQ\omega^n\,. \tag{8}$$

In the event of reaching a steady state, we have

$$\psi^{n+1}=\psi^n\,, \tag{9}$$

and

$$\omega^{n+1}=\omega^n\,. \tag{10}$$

From (5), (6), (9) and (10), we can write

$$\left(1-\Delta t\frac{\partial^2}{\partial x^2}\right)\left(1-\Delta t\frac{\partial^2}{\partial y^2}\right)\psi^{n+1}=\psi^n+\Delta t\omega^n+\left(\Delta t\frac{\partial^2}{\partial x^2}\right)\left(\Delta t\frac{\partial^2}{\partial y^2}\right)\psi^n\,, \tag{11}$$

$$\begin{aligned}&\left(1-\frac{\Delta t}{\mathrm{Re}}\frac{\partial^2}{\partial x^2}+\Delta t\left(\frac{\partial \psi}{\partial y}\right)^n\frac{\partial}{\partial x}\right)\left(1-\frac{\Delta t}{\mathrm{Re}}\frac{\partial^2}{\partial y^2}-\Delta t\left(\frac{\partial \psi}{\partial x}\right)^n\frac{\partial}{\partial y}\right)\omega^{n+1}=\omega^n\\&-\Delta tQ\omega^n+\left(\frac{\Delta t}{\mathrm{Re}}\frac{\partial^2}{\partial x^2}-\Delta t\left(\frac{\partial \psi}{\partial y}\right)^n\frac{\partial}{\partial x}\right)\left(\frac{\Delta t}{\mathrm{Re}}\frac{\partial^2}{\partial y^2}+\Delta t\left(\frac{\partial \psi}{\partial x}\right)^n\frac{\partial}{\partial y}\right)\omega^n.\end{aligned} \tag{12}$$

The algorithm for solving equations (11) and (12) involves a two-level updating. First, we solve the stream function equation. For equation (11), the variable f is introduced such that

$$\left(1-\Delta t\frac{\partial^2}{\partial y^2}\right)\psi^{n+1}=f\,, \tag{13}$$

and

$$\left(1-\Delta t\frac{\partial^2}{\partial x^2}\right)f=\psi^n+\Delta t\omega^n+\left(\Delta t\frac{\partial^2}{\partial x^2}\right)\left(\Delta t\frac{\partial^2}{\partial y^2}\right)\psi^n\,. \tag{14}$$

In equation (14), f is the only unknown and it is first solved at each grid point. Later, the stream function variable (ψ) is advanced into the new time level by using equation (13). The vorticity equation is solved similarly.

2.2. NON-NEWTONIAN CASE

In this section, we again use the stream function (ψ) and vorticity (ω) formulation for the lid-driven flow of an electrically conducting, the steady-state, incompressible, pseudoplastic viscous fluid equations. It has the form

$$\frac{\partial^2\psi}{\partial x^2}+\frac{\partial^2\psi}{\partial y^2}=-\omega\,, \tag{15}$$

$$\begin{aligned}\frac{\partial\psi}{\partial y}\frac{\partial\omega}{\partial x}-\frac{\partial\psi}{\partial x}\frac{\partial\omega}{\partial y}&=\frac{1}{\mathrm{Re}\,\eta(q)}\left\{\frac{\partial}{\partial x}\left(\eta^2(q)\frac{\partial\omega}{\partial x}\right)+\frac{\partial}{\partial y}\left(\eta^2(q)\frac{\partial\omega}{\partial y}\right)\right\}\\&+\frac{1}{\mathrm{Re}}\left\{-4\frac{\partial^2\psi}{\partial x\partial y}\frac{\partial^2\eta(q)}{\partial x\partial y}-\left(\frac{\partial^2\psi}{\partial y^2}-\frac{\partial^2\psi}{\partial x^2}\right)\left(\frac{\partial^2\eta(q)}{\partial y^2}-\frac{\partial^2\eta(q)}{\partial x^2}\right)-Q\omega\right\}.\end{aligned} \tag{16}$$

where $\mathrm{Re}=\dfrac{UL}{\nu}$ is the Reynolds number, $Q=\dfrac{\mu_m^2\sigma H_0^2L}{u\rho}$ is the Chandrasekhar number, q is the shear rate, and $\eta(q)$ is the viscosity. In numerical calculations, we use the Cross model for modeling the viscosity function. It is given as

$$\eta(q)=\eta(\infty)+\frac{\left(\eta(0)-\eta(\infty)\right)}{1+\left(\lambda q\right)^{1-n}}\,.$$

In the Cross Model, $\eta(\infty)$ represents the infinite shear viscosity for very large deformation rates and $\eta(0)$ represents the zero-shear rate viscosity for very small rates of shear. Supposing $n=0.5,\lambda=1,\eta(0)=1$ and $0\le\eta(\infty)\le1$, we obtain shear-thinning or so-called pseudoplastic behavior.

The solutions of equations (15) and (16) are obtained by the same steps as in the Newtonian case.

3. RESULTS AND DISCUSSION

In numerical calculations, we used the algorithm given by Erturk et al. [10]. However, in order to increase the convergence rate, we used the convergence criterion given in [22]. The convergence criterion is based on the following relative-error criterion [22]:

$$\max\left\{\frac{\left|\psi^{n+1}-\psi^{n}\right|}{1+\left|\psi^{n}\right|}\right\}<10^{-6},$$

$$\max\left\{\frac{\left|\omega^{n+1}-\omega^{n}\right|}{1+\left|\omega^{n}\right|}\right\}<10^{-6}\ ,\ \forall n\ .$$

Below is the outline of the algorithm:

Step 1. Input the flow variables.
Step 2. Set the boundary conditions and use a homogeneous initial guess.
Step 3. Solve the streamfunction equation (1) with the spatially factorization method.
Step 4. Solve vorticity equations (2) and (16) with the same method.
Step 5. Check residuals for convergence.
Step 6. Output the residuals.
Step 7. If $max\left\{\frac{|\psi^{n+1}-\psi^{n}|}{1+|\psi^{n}|}\right\}<10^{-6}$, $max\left\{\frac{|\omega^{n+1}-\omega^{n}|}{1+|\omega^{n}|}\right\}<10^{-6}$ then stop iterations.
Step 8. Write computed solutions for output. □

3.1. NEWTONIAN FLUID

In the beginning, our computations had been carried out by solving the lid-driven cavity flow from $\mathrm{Re}=1000$ to $\mathrm{Re}=3000$ on a 128×128 grid mesh. Although a large number of grids had been used, we could not get a steady solution for $\mathrm{Re}=5000$. Many studies in the literature show that the lid-driven cavity flow becomes unstable [23-25]. On the other hand, there are numerous studies [4, 5, 7, 8] providing solutions for a higher Reynolds number, $\mathrm{Re}=10.000$. This was discrepancy. So, we tried to solve the problem for $\mathrm{Re}=5000$ with a larger grid size of 256×256. For this grid size we obtained a steady solution.

We note that all the figures and tables contain the solution of the finest grid size of 401×401 unless otherwise specified.

Table 1 tabulates the maximum stream function value, the vorticity value at the centre of the primary vortex. The centre location of the primary vortex for Newtonian fluid at $\mathrm{Re}=1000$ along with similar results can be found in the literature. In Table 1, among the most significant results, Erturk et al. [10] solved the cavity flow for $\mathrm{Re}=1000$ on three different grid mesh (401×401, 513×513, 601×601).

Table 1. Comparison of the properties of the primary vortex; the maximum stream function value, the vorticity value and the location of the centre, for Re=1000 and Q=0.

Rereference	Grid	ψ	ω	x	y
Erturk et al.[10], 2005	401×401	0.118585	2.062761	0.5300	0.5650
	513×513	0.118722	2.064765	0.5313	0.5645
	601×601	0.118781	2.065530	0.5300	0.5650
Schreiber and Keller[5],1983	121×121	0.11492	2.0112	-	-
	141×141	0.11603	2.0268	0.52857	0.56429
Ghia et al.[8], 1982	129×129	0.117929	2.04968	0.5313	0.5625
Hou et al.[6],1995	256×256	0.1178	2.0760	0.5333	0.5647
Liao et al.[7], 1996	129×129	0.1160	2.0234	0.5313	0.5625
Benjamin et al. [4], 1979	101×101	0.1175	2.044	-	-
Present	128×128	0.115952	2.02482	0.5313	0.5625
	256×256	0.118182	2.05677	0.5313	0.5664
	401×401	0.118626	2.06322	0.5312	0.5661

Going back to Table 1, for $\mathrm{Re}=1000$, our results are in very good agreement with the results of Schreiber and Keller [5], Hou et al. [6] and Erturk et al. [10]. From these comparisons we conclude that even for $\mathrm{Re}=1000$ higher order approximations together with the use of fine grids are necessary to achieve sufficient accuracy.

Table 2. The maximum stream function value, the vorticity value and the location of the centre, for Re=300 and Q=3.

Grid	ψ	ω	x	y
128×128	0.108274	1.678587	0.5234	0.5391
256×256	0.114221	1.764459	0.5195	0.5430
401×401	0.115625	1.784575	0.5187	0.5411

Table 3. The maximum stream function value, the vorticity value and the location of the centre, for Re=1000, Re=3000, Re=5000 and Q=5.

Re	Grid	ψ	ω	x	y
1000	128×128	0.108568	1.784427	0.5313	0.5703
	256×256	0.110634	1.811279	0.5313	0.5664
	401×401	0.111045	1.816832	0.5337	0.5661
3000	128×128	0.105366	1.585758	0.5234	0.5391
	256×256	0.111144	1.666360	0.5195	0.5430
	401×401	0.112508	1.685230	0.5187	0.5411
5000	256×256	0.109889	1.616439	0.5156	0.5352
	401×401	0.112095	1.647471	0.5162	0.5362

Tables 2 and 3 have been documented for the first time. Our results are shown in Figs. 2-4 on three different grid mesh (128×128, 256×256 and 401×401) for $\mathrm{Re}=3000$ and $\mathrm{Re}=5000$; $Q=0$ and $Q=5$, respectively. These results display for interest significant change from $Q=0$ in this paper which has not given before.

128×128, Re=3000, U=1, Q=0

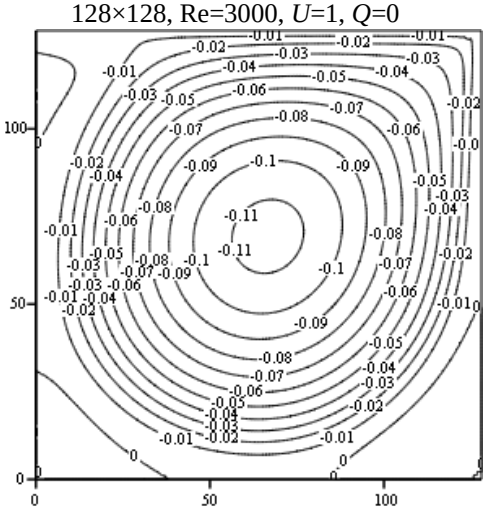

128×128, Re=3000, U=1, Q=5

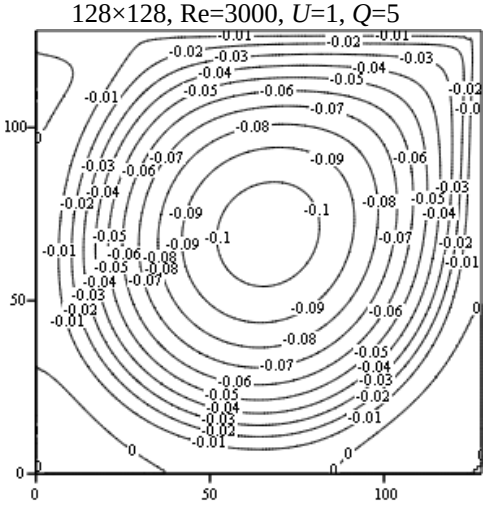

Figure 2. Stream contours of primary vortices for Re=3000 on a 128×128 grid mesh.

256×256, Re=5000, U=1, Q=0

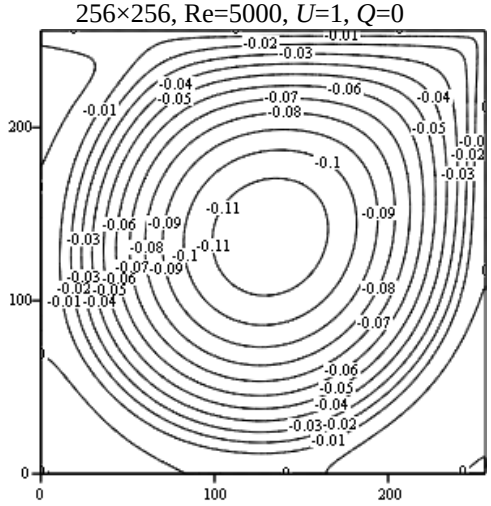

256×256, Re=5000, U=1, Q=5

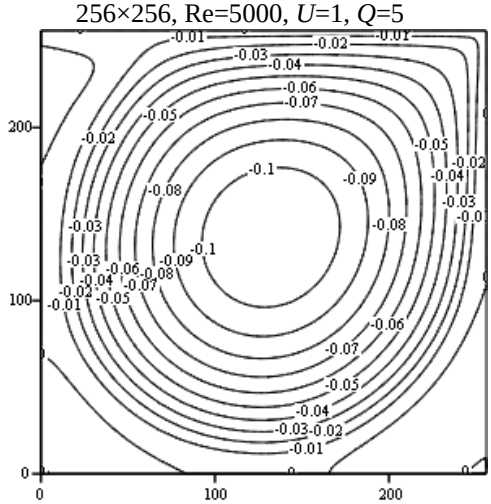

Figure 3. Stream contours of primary vortices for Re=5000 on a 256×256 grid mesh.

401×401, Re=5000, U=1, Q=0

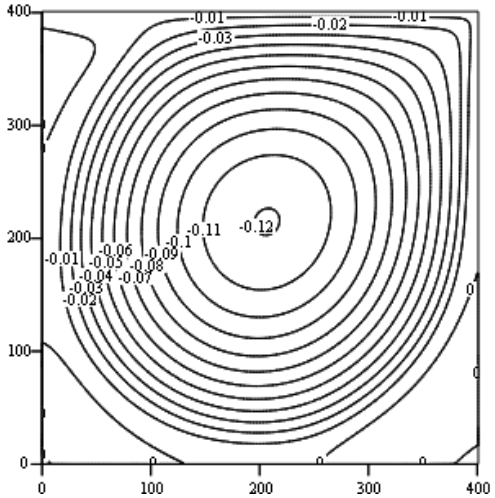

401×401, Re=5000, U=1, Q=5

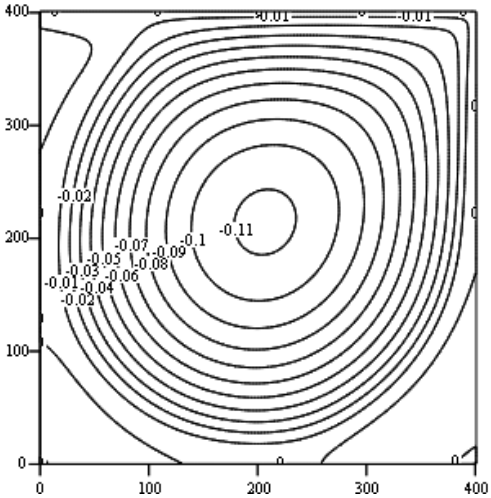

Figure 4. Stream contours of primary vortices for Re=5000 on a 401×401grid mesh.

Figs. 2-4 show that the steady solution gives one large symmetric rotating vortex filling the whole flow domain. The streamlines become more circular around the vortex centre

located in the middle of the cavity. These figures exhibit the formation of the counter-rotating secondary vortices that appear as the Reynolds number increases. Note that the streamlines are reduced for $Q=5$. From these comparisons, we conclude that even for $\mathrm{Re}=1000$, the use of fine grids is necessary to get sufficient accuracy.

3.2. NON-NEWTONIAN FLUID

In this section, we present numerical results for the lid-driven hydromagnetic flow of non-Newtonian pseudoplastic fluids. If we take the Chandresekhar number $Q=0$, then it coincides with the lid-driven flow of non-Newtonian pseudoplastic fluids [26]. Streamlines corresponding to $Q=3$ and $\mathrm{Re}=300$; $Q=5$, $Q=10$ and $\mathrm{Re}=1000$, $\mathrm{Re}=1500$, $\mathrm{Re}=2000$ are given for non-Newtonian pseudoplastic fluids in the Figs. 5-19, respectively.

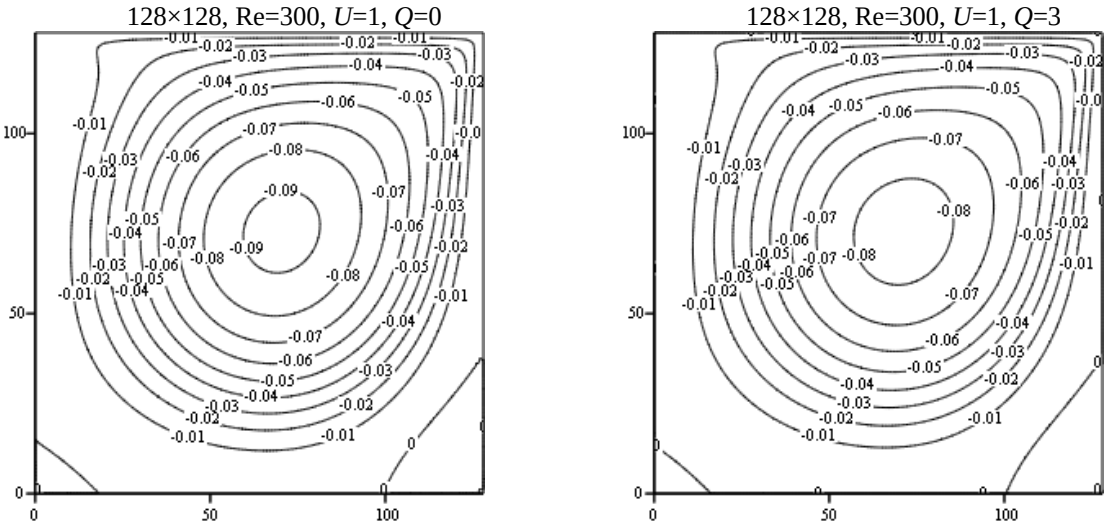

Figure 5. Stream contours of primary vortices for Re=300 on a 128×128 grid mesh.

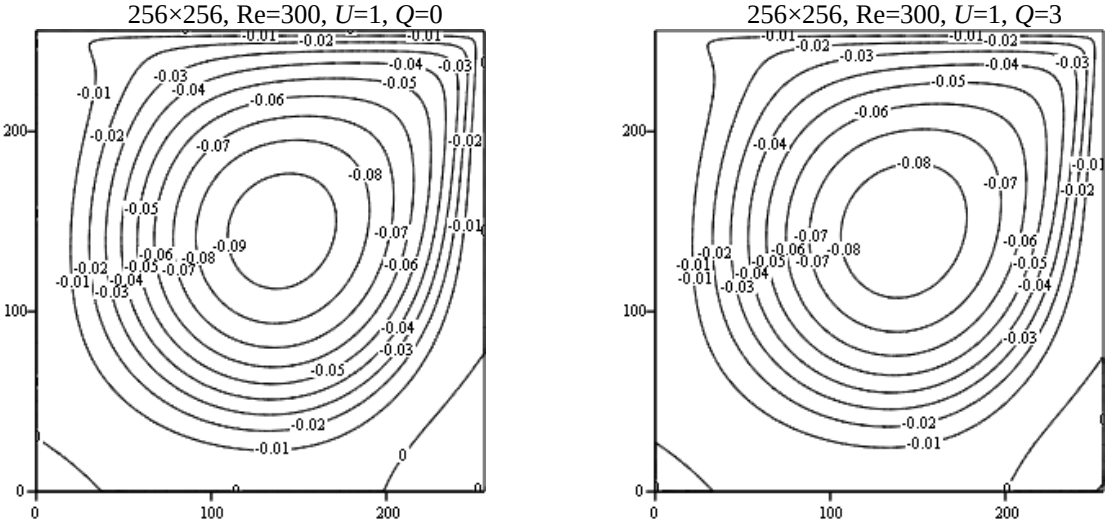

Figure 6. Stream contours of primary vortices for Re=300 on a 256×256 grid mesh.

401×401, Re=300, *U*=1, *Q*=0

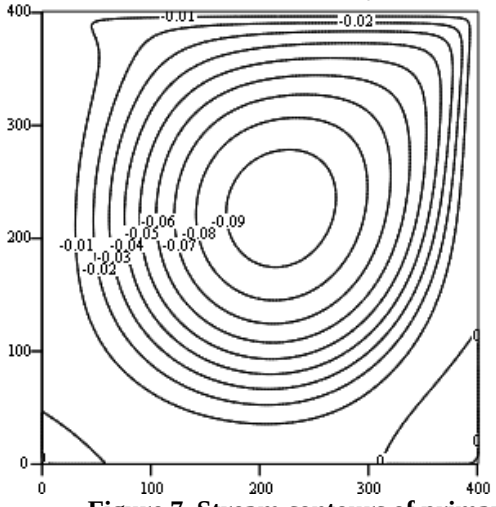

401×401, Re=300, *U*=1, *Q*=3

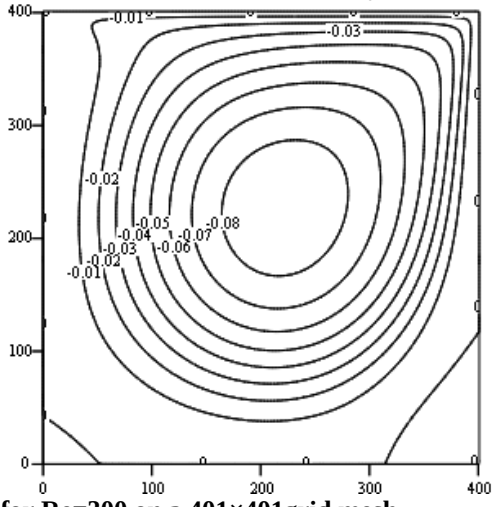

Figure 7. Stream contours of primary vortices for Re=300 on a 401×401grid mesh.

128×128, Re=1000, *U*=1, *Q*=0

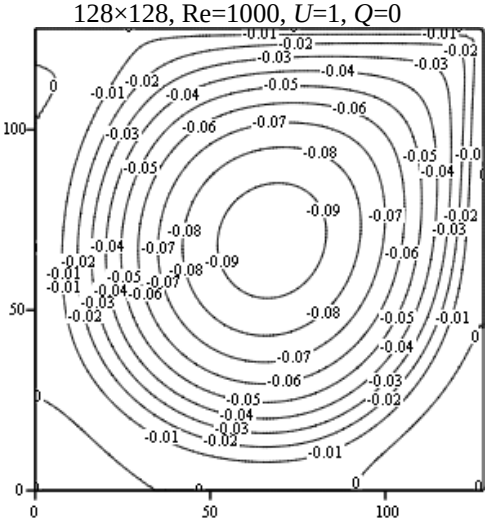

128×128, Re=1000, *U*=1, *Q*=5

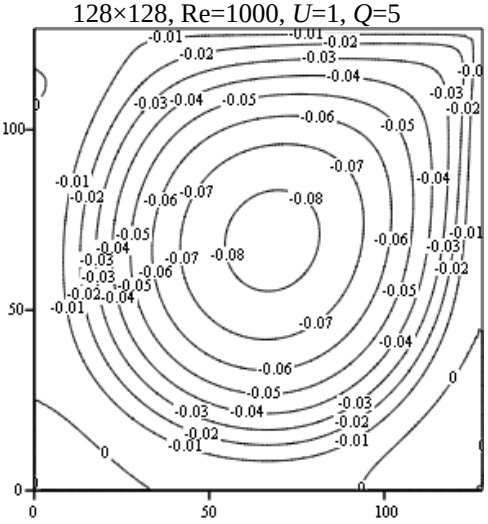

Figure 8. Stream contours of primary vortices for Re=1000 on a 128×128 grid mesh.

256×256, Re=1000, *U*=1, *Q*=0

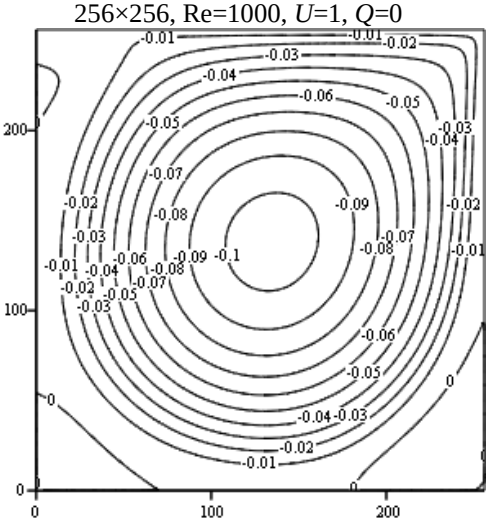

256×256, Re=1000, *U*=1, *Q*=5

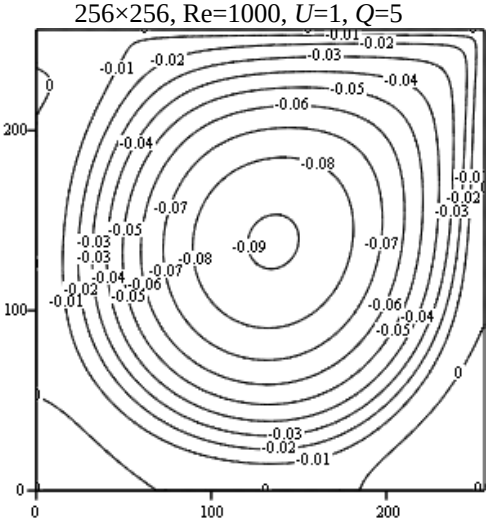

Figure 9. Stream contours of primary vortices for Re=1000 on a 256×256 grid mesh.

401×401, Re=1000, U=1, Q=0

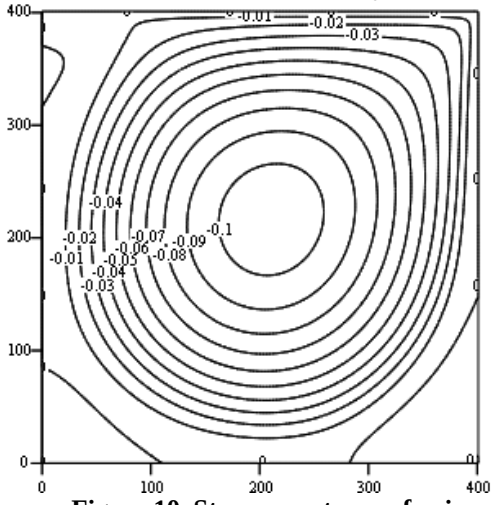

401×401, Re=1000, U=1, Q=5

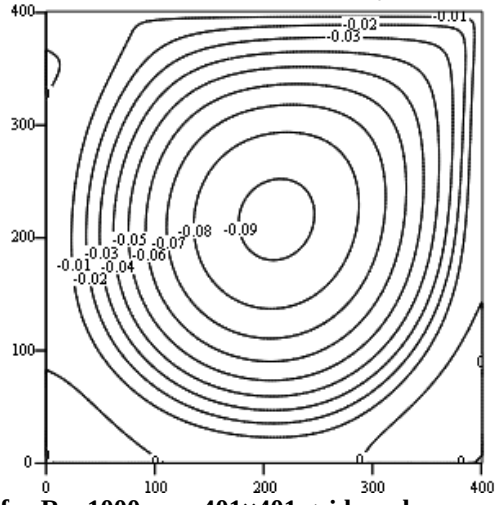

Figure 10. Stream contours of primary vortices for Re=1000 on a 401×401 grid mesh.

128×128, Re=2000, U=1, Q=0

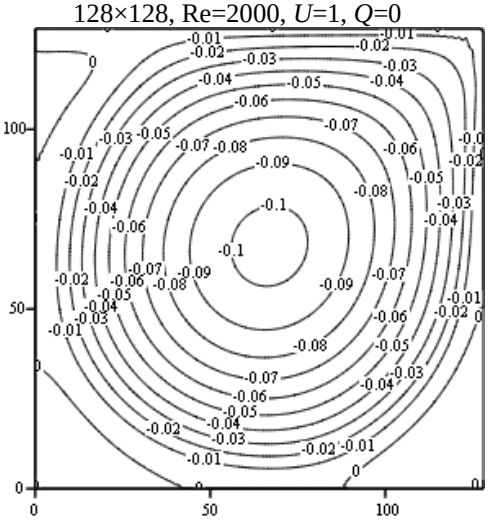

128×128, Re=2000, U=1, Q=5

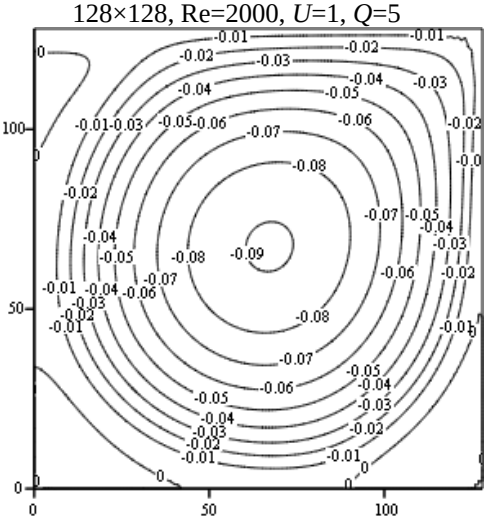

Figure 11. Stream contours of primary vortices for Re=2000 on a 128×128 grid mesh.

256×256, Re=2000, U=1, Q=0

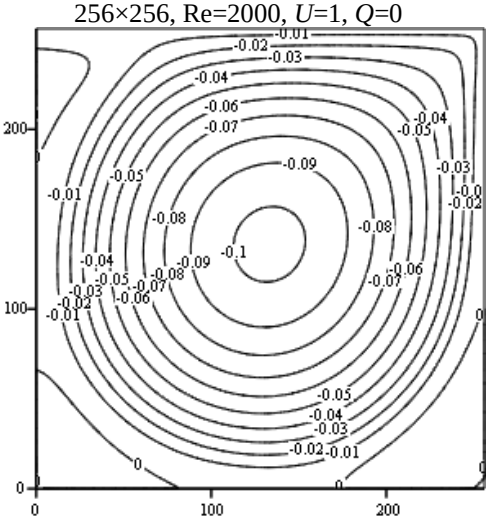

256×256, Re=2000, U=1, Q=5

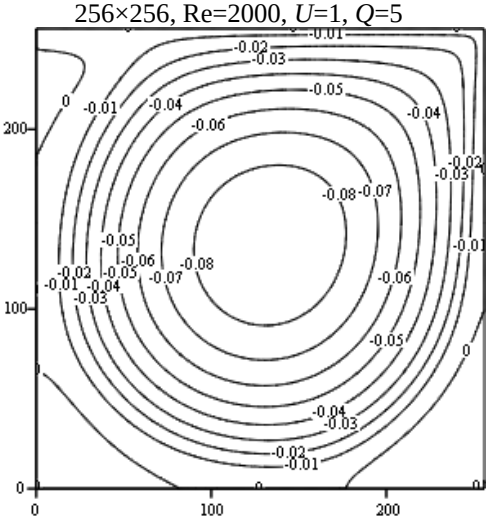

Figure 12. Stream contours of primary vortices for Re=2000 on a 256×256 grid mesh.

401×401, Re=2000, U=1, Q=0

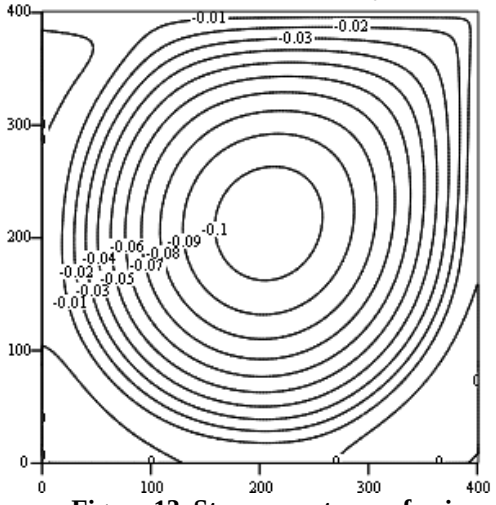

401×401, Re=2000, U=1, Q=5

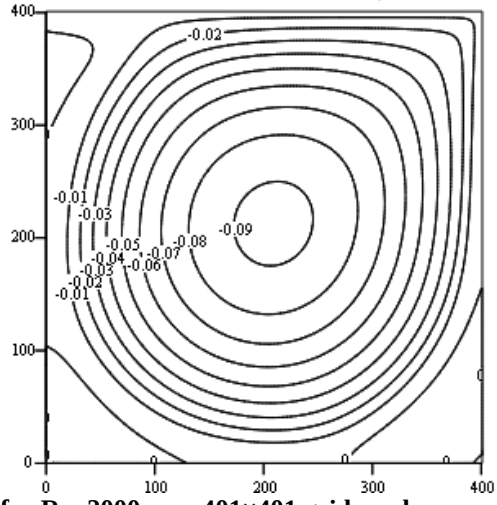

Figure 13. Stream contours of primary vortices for Re=2000 on a 401×401 grid mesh.

128×128, Re=1000, U=1, Q=0

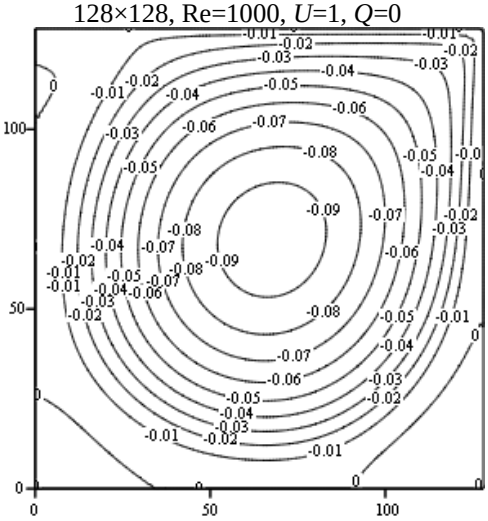

128×128, Re=1000, U=1, Q=10

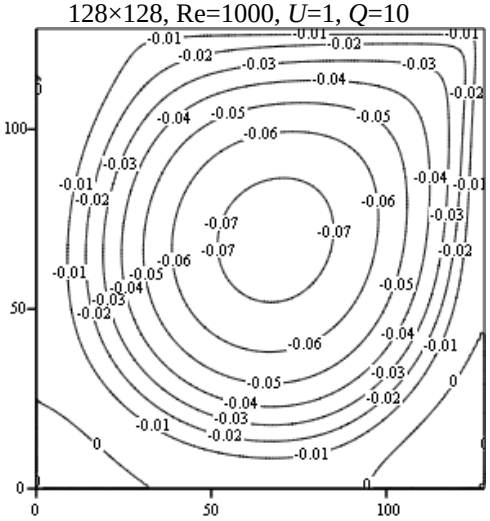

Figure 14. Stream contours of primary vortices for Re=1000 on a 128×128 grid mesh.

256×256, Re=1000, U=1, Q=0

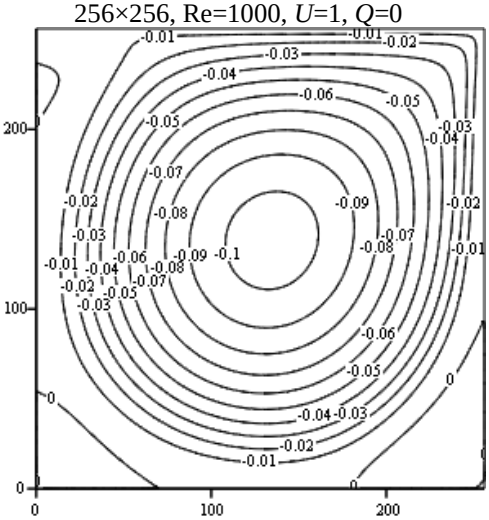

256×256, Re=1000, U=1, Q=10

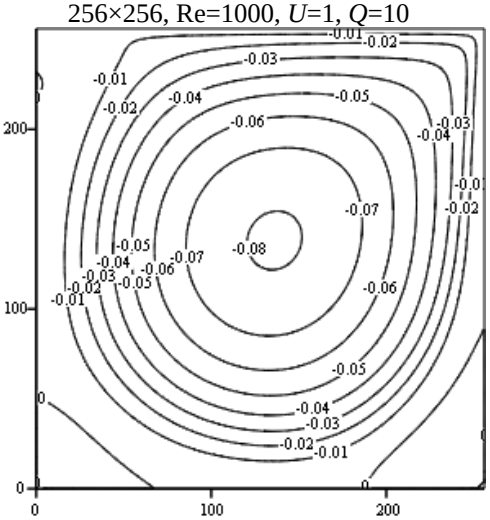

Figure 15. Stream contours of primary vortices for Re=1000 on a 256×256 grid mesh.

401×401, Re=1000, U=1, Q=0

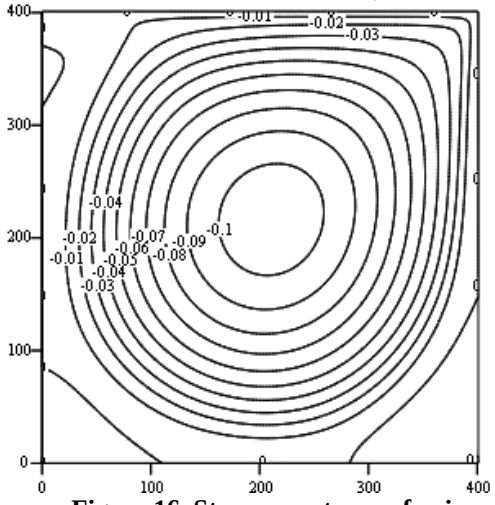

401×401, Re=1000, U=1, Q=10

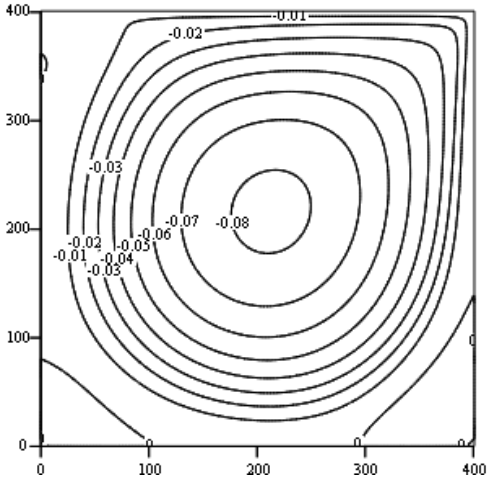

Figure 16. Stream contours of primary vortices for Re=1000 on a 401×401 grid mesh.

128×128, Re=2000, U=1, Q=0

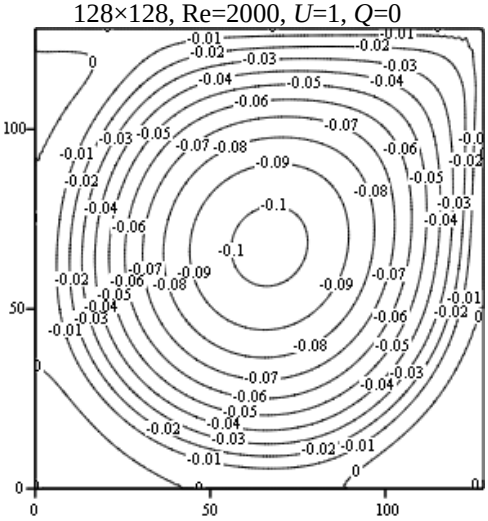

128×128, Re=2000, U=1, Q=10

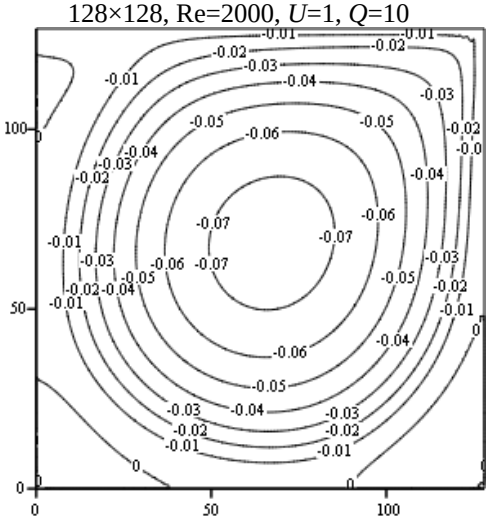

Figure 17. Stream contours of primary vortices for Re=2000 on a 128×128 grid mesh.

256×256, Re=2000, U=1, Q=0

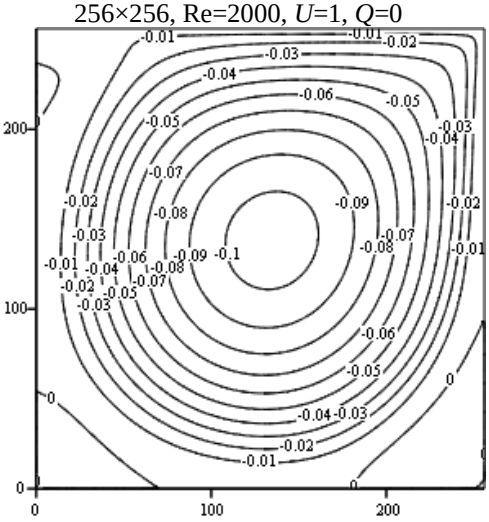

256×256, Re=2000, U=1, Q=10

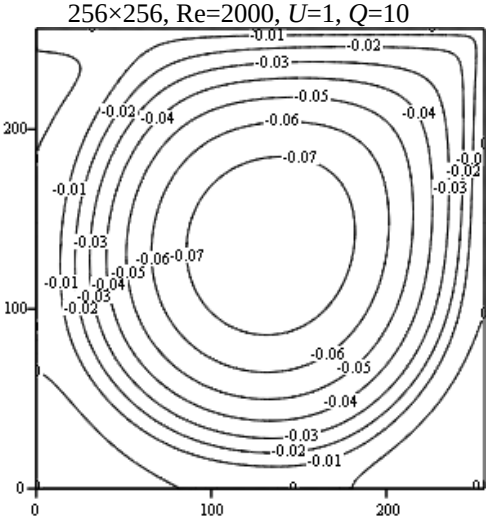

Figure 18. Stream contours of primary vortices for Re=2000 on a 256×256 grid mesh.

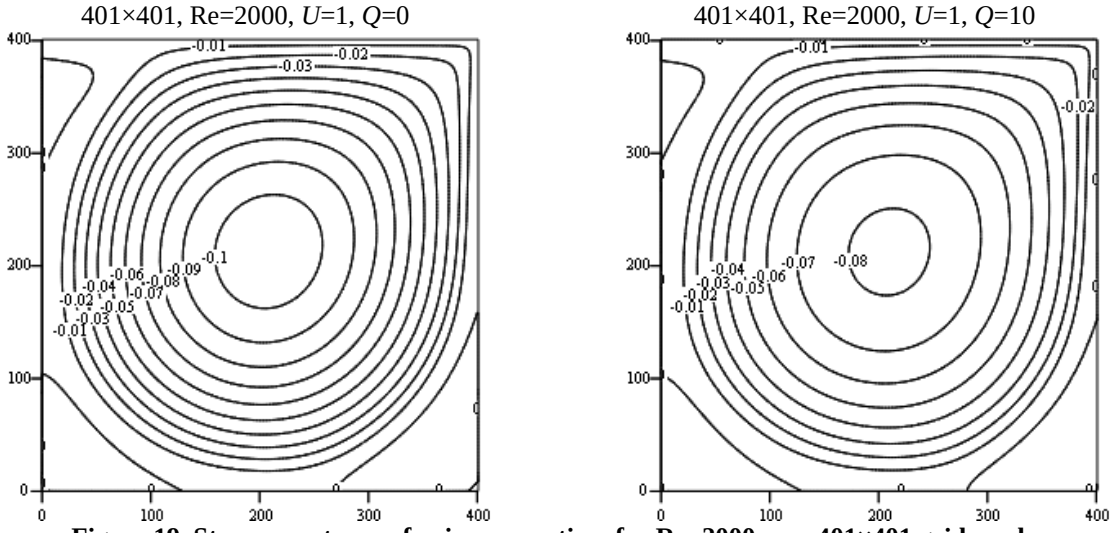

Figure 19. Stream contours of primary vortices for Re=2000 on a 401×401 grid mesh.

The streamline contours obtained by using three different grid mesh (128×128, 256×256, 401×401) are respectively given in Figs. 5-7. As shown in these figures, a main vortex is observed in the cavity region for both the cases $Q = 0$ and $Q = 3$. Additionally, the secondary vortex appears in the bottom right and left corner. When the Chandrasekhar number increases, the intensity of the streamlines decreases. Furthermore, as number of grids rises, the streamline contours become smoother. Figs. 8-19 indicate stream function contours of three different grid solutions for various Reynolds and Chandrasekhar numbers. These figures exhibit the formation of secondary vortices in the top left corner which appear as the Reynolds and Chandrasekhar numbers increase.

Table 4. The maximum stream function value, the vorticity value and the location of the centre, for Re=300 and Q=3.

Grid	ψ	ω	x	y
128×128	0.084620	1.457197	0.5547	0.5703
256×256	0.114221	1.764459	0.5195	0.5430
401×401	0.115625	1.784575	0.5187	0.5411

Table 5. The maximum stream function value, the vorticity value and the location of the centre, for Re=1000, Re=2000 and Q=5.

Re	Grid	ψ	ω	x	y
1000	128×128	0.083530	1.225889	0.5313	0.5391
	256×256	0.091099	1.319609	0.5273	0.5391
	401×401	0.092602	1.338352	0.5287	0.5411
2000	128×128	0.090913	1.275941	0.5234	0.5234
	256×256	0.089411	1.254815	0.5234	0.5313
	401×401	0.092739	1.297914	0.5212	0.5312

Table 6. The maximum stream function value, the vorticity value and the location of the centre, for Re=1000, Re=2000 and Q=10.

Re	Grid	ψ	ω	x	y
1000	128×128	0.074346	0.987171	0.5313	0.5391
	256×256	0.081025	1.057136	0.5313	0.5391
	401×401	0.082358	1.071141	0.5312	0.5387
2000	128×128	0.075017	0.974716	0.5234	0.5313
	256×256	0.079375	0.994980	0.5234	0.5313
	401×401	0.082316	1.027705	0.5237	0.5312

The Tables 4-6 have been documented for the first time and these results show for interest significant change from the $Q = 0$ in this paper which has not given before.

4. CONCLUSIONS

Numerical solutions for the 2D steady-state incompressible hydro magnetic lid-driven cavity flow have been presented and documented for the first time. The flow equations in stream function and vorticity formulation for weakly electrically conducting Newtonian and non-Newtonian liquids are solved computationally by using numerical methods. In this numerical approach the stream function and vorticity equations are solved separately by using pseudo time derivative. For each equation, the numerical formulation requires the solution of two tridiagonal systems. This allows the use of large grid meshes easily. We used a fine grid mesh of 401×401. The method proved to be very effective on flow problems that require high accuracy on very fine grid meshes [27, 28].

Stable solutions are found for high Reynolds numbers in Newtonian flow, and for high Chandrasekhar numbers in non-Newtonian flow. This is the most important difference between Newtonian and non-Newtonian cases.

The main parameters expected to affect the stability of the flow solution are the Reynolds and Chandrasekhar numbers. As the Chandrasekhar number increases, the streamlines become weaker in the central part of the cavity. When the Reynolds number increases, the vortex tends to move in the direction of the moving plate.

Also, our computations show that fine grid mesh is necessary to obtain a steady solution. The presented results were found to agree very well with the published numerical solutions for Newtonian fluids in the literature [4, 5, 7- 10].

Finally, the increase in studies on non-Newtonian fluids is very important for the comparison of the available data in the literature.

Acknowledgement: *The authors thank the referee for helpful suggestions.*

REFERENCES

[1] Chandrasekhar, S., *Hydrodynamic and Hydromagnetic Stability*, Oxford University Press, Oxford, 1961.
[2] Danielson, R.E., *Astrophysical Journal*, **134**, 289, 1961.
[3] Unno, W., *Basic plasma processes on the sun*, Kluwer Academic Publishers, Netherlands, 1990.
[4] Benjamin, A.S., Denny, V.E., *J. Comp. Physics*, **33**(3), 340, 1979.
[5] Schreiber, R., Keller, H.B., *J. Comp. Physics*, **49**(2), 310, 1983.
[6] Hou, S., Zou, Q., Chen, S., Doolen, G., Cogley, A.C., *J. Comp. Physics*., **118**(2), 329, 1995.
[7] Liao, S.J., Zhu, J.M., *Int. J. Numer. Methods Fluids*, **22**(1), 1, 1996.
[8] Ghia, U., Ghia, K.N., Shin, C.T., *J. Comp. Physics*., **48**(3), 387, 1982.
[9] Rubin, S.G., Khosla, P.K., *Computers and Fluids*, **9**(2), 163, 1981.
[10] Erturk, E., Corke, T.C., Gökçöl, C., *Int. J. Numer. Meth. Fluids*, **48**(7), 747, 2005.
[11] Gunzburger, M.D., Meir, A.J., Peterson, J.S., *Math. Comput.*, **56**(194), 523, 1991.

[12] Hasler, U., Schneebeli, A., Schötzau, D., *Appl. Numer. Math*., **51**(1), 19, 2004.
[13] Salama, F.A., *Appl. Math. and Mech.,* **31**(8), 963, 2010
[14] Siddheshwar, P.G., Ramachandramurthy, V., Uma, D., *Int. J. Engng Sci.*, **49**(10), 1078, 2011.
[15] Raisi, A., Qanbary, A., *Chinese Journal of Mechanical Engineering,* **29**, 1235, 2016.
[16] Venkatachalappa, M., Younghae, D., Sankar, M., *Int. J. Engg. Sci.*, **49**(3), 262, 2011.
[17] Hasanpour, A., Farhadi, M., Sedighi, K., Ashorynejad, H.R., *Int. J. Numer. Meth. Fluids*, **70**(7), 886, 2012.
[18] Mirza, I.A., Abdulhameed, M., Shafie, S., *Appl. Math. and Mech*., **38**(3), 379, 2017.
[19] Aydın, S.H., Neslitürk, A.I., Tezer, S.M., *Int. J. Numer. Meth. Fluids*; **62**(2), 188, 2010.
[20] He, Y.N., Li, J., *Comput. Methods Appl. Mech. Engrg.*, **198**(15-16), 1351, 2009.
[21] Xu, H., He, Y.N., *J. Comput. Phys.*, **232**(1), 136, 2013.
[22] Demir, H., *Appl. Math. And Comp.*, **166**(1), 64, 2005.
[23] Fortin, A., Jardak, M., Gervais, J.J., Pierre, R., *Int. J. Numer. Meth. Fluids*, **24**(11), 1185, 1997.
[24] Peng, Y.F., Shiau, Y.H., Hwang, R.R., *Computers and Fluids,* **32**(3), 337, 2003.
[25] Poliashenko, M., Aidun, C.K., *Journal of Computational Physics,* **121**(2), 246, 1995.
[26] Demir, H., Şahin, S., *Turkish Journal of Mathematics and Computer Science*, **1**, 14, 2013.
[27] Erturk, E., Corke, T.C., *Journal of Fluid Mechanics*, **444**, 383, 2001.
[28] Erturk, E., Haddad, O.M., Corke, T.C., *AIAA Journal*, **42**(11), 2254, 2004.
[29] Smith, G.D., *Numerical solution of partial differential equations by finite difference method.,* Oxford University Press, New York, 1978.